Vibrations modelling at LBTO utilizing telemetry data

María Coronel[a], Pedro Escárate[b,c], , Julian C. Christou[d], John M. Hill[d], Gustavo Rahmer[d], Rodrigo Carvajal[a], and Juan C. Agüero[a]

[a]Electronics Engineering Department, Universidad Técnica Federico Santa María, Valparaíso, Chile;
[b]Instituto de Electricidad y Electrónica, Facultad de Ciencias de la Ingeniería, Universidad Austral, Valdivia, Chile;
[c]Núcleo Milenio de Formación Planetaria - NPF, Chile;
[d]Large Binocular Telescope Observatory, Steward Observatory, Tucson, AZ 85546, USA.

ABSTRACT

It is widely accepted that the non-turbulent perturbations in modern telescopes arise from the instrumentation systems, such as fans and cooling pumps, and from the mechanical vibrations induced by the wind or the telescope tracking. In order to develop a properly control law to mitigate the vibrations effects, an accurate model of all the mechanical vibrations is needed. In this paper, we model these vibrations as a sum of continuos-time damped oscillators (the equivalent transfer function of discrete-time autoregressive second-order models) and we estimate the oscillators parameters from discrete-time data based on Maximum Likelihood method. Finally, we utilize our proposed method to estimate the vibrations frequency peaks at the LBTO.

Keywords: Vibration analysis, Active or adaptive optics

1. INTRODUCTION

In Adaptive Optics (AO) systems, a deformable mirror is utilized in order to compensate the wavefront distortions caused by the atmospheric turbulences, mechanical vibrations, wind shake, and tracking errors on the astronomical images that are sensed by the wavefront sensor, see e.g.[1,2]

Mechanical vibrations have been a subject of study in different areas, such as AO,[1,3–6] Signal Processing and Communications.[7] In particular, the main interest in mechanical vibrations within the AO community is due to the great sensitivity that AO systems exhibit to the vibrations acting in the propagation of the science light. This sensitivity has led to the identification of the main sources of vibrations, such as the wind and elements within the instrumentation of the system (e.g. fans and cooling pumps), and the implementation of control laws to effectively mitigate those vibrations.[2,4,8,9]

On the other hand, for the development and implementation of adequate control laws, accurate models of the system are usually needed. In AO systems, a model that has been widely used in the literature is shown in Fig. 1, where the AO closed-loop system consists of a wavefront sensor (WFS), a deformable mirror (DM), and a controller (K), see e.g.,[1,7] and φ^{cor}, φ^{cor} and φ^{res} are the amplitudes for the total disturbance phase, the correction phase, and the residual phase, respectively.

A commonplace model for each one of the vibrations is the discrete-time second order autoregressive system, see e.g.,[1,4] yielding a stationary time series. These AR(2) systems, when excited by a white noise, are expected to exhibit large peaks at the vibrations frequencies in their power spectral density plots. On the other hand, a simple technique for estimating the frequencies associated with the mechanical vibrations in AO systems is based on the well known periodogram, see e.g.[8,9] The periodogram is, in general, a low complexity technique that is widely utilized for estimating the power spectral density of a time series.[10] However, the periodogram is only a reliable and accurate estimator when the time series corresponds to sinusoidal waves at fixed frequencies that are corrupted by additive noise. Moreover, "stationary time series are characterized by random changes of

Further author information: (Send correspondence to P. Escárate)
P. Escárate: e-mail: pedro.escarate@uach.cl

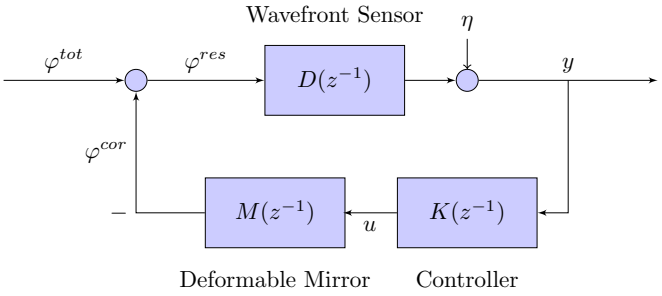

Figure 1. Block diagram for an AO closed-loop system.

frequency, amplitude, and phase. For this type of series, the sample spectrum, i.e. the periodogram, fluctuates wildly and is not capable of any meaningful interpretation" [10, pag. 37]. Thus, a more adequate method for modelling the vibrations is needed.

In[5] an early work modelling the vibrations as continuos-time harmonic oscillators driven by noise was developed. Based on,[11] the estimation of the parameters associated with the oscillators was carried out via the computation of the prediction error and the Kalman filter within the Maximum Likelihood (ML) framework.

In this paper, we model the vibrations as continuous-time damped oscillator with initial condition different from zero. The estimation of the damped oscillators parameters is carried out from discrete-time samples utilizing ML.[12–14] The corresponding optimization problem is solved utilizing a local optimization algorithm, namely Interior Point through the Matlab function `fmincon`. We illustrate the behavior and benefits of our technique via numerical simulations, and then we utilize the proposed method in on-sky data measurements of the WFS and the accelerometers network data (OVMS[15,16]) of the Large Binocular Telescope Observatory (LBTO). The results show that the frequency vibrations peaks (continuous-time) can be adequately estimated using continuos-time damped oscillators from the corresponding discrete-time samples.

2. SYSTEM MODEL

The system of interest can be modeled as a linear combination of continuous-time damped oscillators driven by noise:

$$y(t) = \sum_{i=1}^{m} \frac{\beta_i}{\mathbf{p}^2 + 2\zeta_i\alpha_i\mathbf{p} + \alpha_i^2}\dot{\omega}_i(t), \tag{1}$$

where $y(t)$ is the system output, β_i is the oscillator gain of the i-th damped oscillator, α_i is the vibration frequency, ζ_i is the damping coefficient, m is the number of oscillators, $\mathbf{p} = \frac{d}{dt}$ and $\dot{\omega}(t)$ is the (continuous-time) zero-mean white gaussian noise. We assume that the noises $\dot{\omega}_i$ are not correlated with variance $\sigma_i^2 = 1$.

2.1 State Space Model

The model in (1) can be represented in state-space form as a continuous-time autoregressive system (CAR):

$$\dot{x}(t) = Ax(t) + \kappa\dot{w}(t), \tag{2}$$
$$y(t) = Cx(t), \tag{3}$$

where $A \in \mathbb{R}^{2m\times 2m}$, $\kappa \in \mathbb{R}^{2m\times 1}$ and $C \in \mathbb{R}^{1\times 2m}$ are given by:

$$A = \begin{bmatrix} 0 & 1 & 0 & \cdots & 0 \\ -\alpha_1^2 & -2\zeta_1\alpha_1 & 0 & \cdots & 0 \\ \vdots & \vdots & \ddots & \vdots & \vdots \\ 0 & 0 & \cdots & 0 & 1 \\ 0 & 0 & \cdots & -\alpha_m^2 & -2\zeta_n\alpha_m \end{bmatrix}, \tag{4}$$

$$\kappa = \left[\begin{array}{cc|cc|c|cc} 0 & \beta_1 & 0 & \beta_2 & \cdots & 0 & \beta_m \end{array}\right]^T, \tag{5}$$

$$C = \left[\begin{array}{cc|cc|c|cc} 1 & 0 & 1 & 0 & \cdots & 1 & 0 \end{array}\right]. \tag{6}$$

2.2 Equivalent Discrete-Time Model

Considering instantaneous sampling, non-zero initial conditions, and sampling period Δ, the equivalent discrete-time state-space model for (1) is given by:

$$x_{k+1} = A_d x_k + v_k, \tag{7}$$

$$x(0) = x_0, \tag{8}$$

$$y_k = Cx_k, \tag{9}$$

$$y_k = CA_d^k x_0 + \sum_{l=0}^{k-1} CA_d^{k-l-1} v_l, \tag{10}$$

where $A_d = e^{A\Delta}$, $x_k = x(t_k)$, $y_k = y(t_k)$, $v_k = v(t_k) = \int_0^\Delta e^{A\eta}\kappa\dot{\omega}(t_{k+1}-\eta)d\eta$ is a zero-mean white Gaussian noise with variance Q_d, and x_0 is the initial condition.The matrices A_d and Q_d can be computed from an extended exponential matrix.[5]

Finally the vector of parameters to estimate is:

$$\theta = \left[\begin{array}{ccc} \vec{\alpha}^T & \vec{\zeta}^T & \vec{\beta}^T \end{array}\right]^T, \tag{11}$$

where $\vec{\alpha} = [\alpha_1 \quad \alpha_2 \quad \cdots \quad \alpha_m]^T$, $\vec{\zeta} = [\zeta_1 \quad \zeta_2 \quad \cdots \quad \zeta_m]^T$, and $\vec{\beta} = [\beta_1 \quad \beta_2 \quad \cdots \quad \beta_m]^T$.

3. MAXIMUM LIKELIHOOD (ML) ESTIMATION

A widely used method in estimation problems is ML, where the goal is to obtain a set of parameters that best explain the collected data, i.e. the parameters that make the given data most probable in the sense that the likelihood function $p(y_{0:N-1}|\theta)$, for the data of size N, is maximized.[12] Thus, the following optimization problem should be solved:

$$\hat{\theta}_{\mathrm{ML}} = \arg\max_\theta L_N(\theta). \tag{12}$$

Equivalently, since the logarithm function is a monotonically increasing function, we can obtain the ML estimator from

$$\hat{\theta}_{\mathrm{ML}} = \arg\min_\theta \; -\ell_N(\theta), \tag{13}$$

where $\ell_N(\theta) = \log\left[L_N(\theta)\right]$ is the log-likelihood function.

On the other hand, in the System Identification community, it is well known that the log-likelihood function can be computed from the decomposition of the prediction error as (see e.g.[12,13]).

$$\ell_N(\theta) = -\frac{1}{2}\sum_{k=1}^{N}\frac{\varepsilon_k^2(\theta)}{\Lambda_k(\theta)} - \frac{1}{2}\sum_{k=1}^{N}\log\left[\Lambda_k(\theta)\right], \tag{14}$$

where $\varepsilon_k(\theta)$ is the prediction error defined by

$$\varepsilon_k(\theta) = y_k - CA_d^k x_0 - \mathbb{E}\left\{y_k | y_{0:k-1}, \theta\right\}, \tag{15}$$

and

$$\Lambda_k(\theta) = \mathbb{E}\left\{\varepsilon_k^2 | y_{0:k-1}, \theta\right\} \tag{16}$$

is the prediction error variance, being both directly obtained from the Kalman filter[13] assuming that y_0 is normally distributed with mean $\hat{y}_{0|-1}(\theta)$ and variance $\Sigma_{0|-1}(\theta)$. Then $\varepsilon_k(\theta)$ and $\Lambda_k(\theta)$ are computed as

$$\varepsilon_k(\theta) = y_k - CA_d^k x_0 - C\hat{x}_{k|k-1}, \tag{17}$$

$$\Lambda_k(\theta) = C\Sigma_{k|k-1}C^T. \tag{18}$$

On the other hand, the log-Likelihood function ($\ell_N(\theta)$) for the damped oscillator in (1) is non-convex. Then, it is necessary to use numerical methods to solve the minimization problem. Here, we use a local optimization algorithm based on the Interior-Point Optimization method[17] through the Matlab function `fmincon`.

4. NUMERICAL EXAMPLES

4.1 Simulated Data

In order to validate our approach, we consider a continuous-time damped oscillator system given by:

$$y(t) = \frac{\beta}{\mathbf{p}^2 + 2\zeta\alpha\mathbf{p} + \alpha^2}\dot{\omega}(t). \tag{19}$$

For the simulation we use one of the typical vibration frequencies for an AO system , namely $\alpha = 20\ Hz$,[4] with $\zeta = 0.1$ and $\beta = 1$. The sample time is $\Delta = 100\ \mu s$, the sample length is $N = 10000$, and we run 100 Monte Carlo simulations. We assume that the initial condition of the state is $x_0 = [0.2 \quad 0.1]^T$ and thus the vector of parameters to identify is $\theta = [\alpha \ \ \zeta \ \ \beta]^T$.

The simulation results show that the parameters estimation are very accurate, exhibiting a very small variance. The simulation results are summarized on Table 1.

4.2 Real Data

For the modelling of vibrations peaks at the LBTO, on-sky data from the WFS and OVMS system were recorded during March 31, 2018 observing run. For the estimation, 12 damped oscillators were considered, and the data was separated into the x-axis and y-axis movement of the focal point, In Fig. 2 we show the estimated power spectral density (PSD) of movement on the x-axis of the focal point that was captured by the OVMS system. The peaks in the estimated PSD were superimposed with the oscillators frequencies that were estimated using the approach presented in this paper. It is clear that the main peaks of the estimated PSD are identified as such from the continuous-time damped oscillators model here proposed.

In Fig. 3 we show the estimated power spectral density (PSD) of movement on the y-axis of the focal point that was captured by the OVMS system and the oscillators frequencies that were estimated using the approach presented in this paper.

The estimation results are summarized in Table 2 for the 12 oscillators on the x-axis and in Table 3 for the y-axis.

Table 1. Statistics of the estimation of the parameters.

θ	Real Value	Estimated Value
α	20	20.0053 ± 0.0222
ζ	0.1	0.0998 ± 0.0011
β	1	0.9991 ± 0.0067

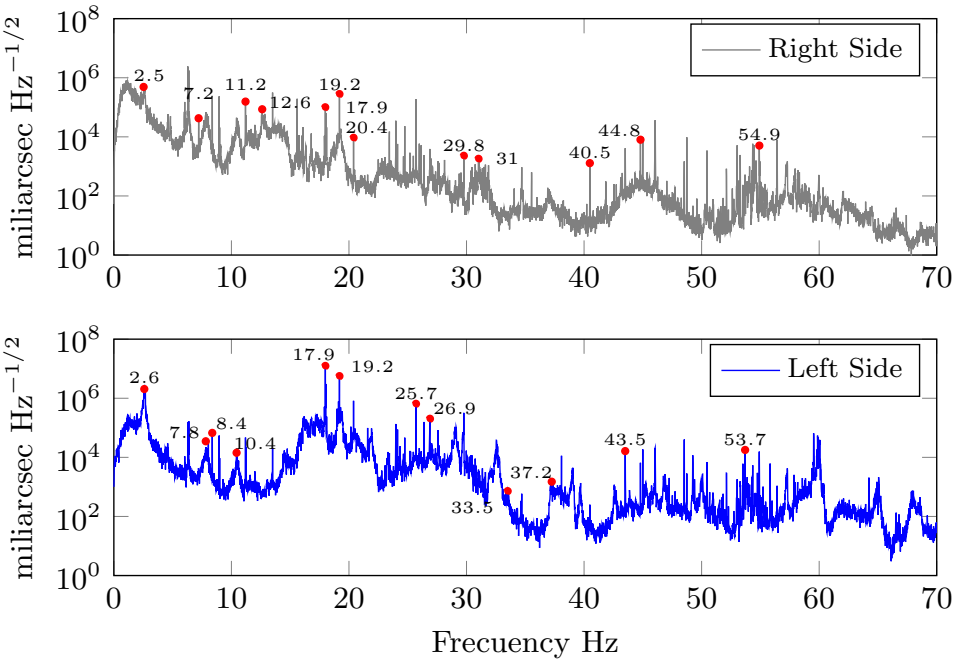

Figure 2. PSD of movement on x-axis of the focal point captured by the OVMS system.

Table 2. Estimation of movement on x-axis of the focal point captured by the OVMS system.

	Right side			Left side		
i	$\hat{\alpha}$	$\hat{\zeta}$	$\hat{\beta}$	$\hat{\alpha}$	$\hat{\zeta}$	$\hat{\beta}$
1	2.42	0.287	70.99	2.99	0.256	52.52
2	7.57	0.042	69.94	7.21	0.001	44.54
3	12.93	0.001	93.99	8.48	0.988	46.29
4	11.47	0.015	31.19	10.86	0.002	39.56
5	18.13	0.002	0.50	19.19	0.015	87.89
6	20.01	0.055	78.56	18.13	0.004	83.83
7	19.04	0.245	69.97	25.48	0.012	32.59
8	29.81	0.139	9.00	26.79	0.001	0.51
9	31.58	0.388	39.32	33.66	0.987	9.91
10	39.70	0.988	5.06	37.35	0.001	6.54
11	44.49	0.053	127.64	43.08	0.001	43.23
12	54.91	0.001	27.87	53.75	0.002	18.72

Table 3. Estimation of movement on y-axis of the focal point captured by the OVMS system.

	Right side			Left side		
i	$\hat{\alpha}$	$\hat{\zeta}$	$\hat{\beta}$	$\hat{\alpha}$	$\hat{\zeta}$	$\hat{\beta}$
1	3.78	0.989	87.81	2.82	0.001	23.88
2	2.08	0.001	27.06	3.95	0.597	47.04
3	11.79	0.001	26.34	9.27	0.267	110.28
4	8.82	0.001	79.77	14.20	0.990	0.50
5	14.59	0.086	177.88	18.01	0.016	144.52
6	25.26	0.001	0.50	25.03	0.073	79.85
7	22.04	0.002	97.74	25.79	0.019	58.82
8	14.00	0.307	164.29	39.99	0.163	66.72
9	27.78	0.014	1.39	33.69	0.012	28.12
10	36.63	0.047	116.68	42.61	0.047	48.59
11	42.94	0.001	55.53	42.22	0.001	0.51
12	34.04	0.062	64.43	53.16	0.032	54.96

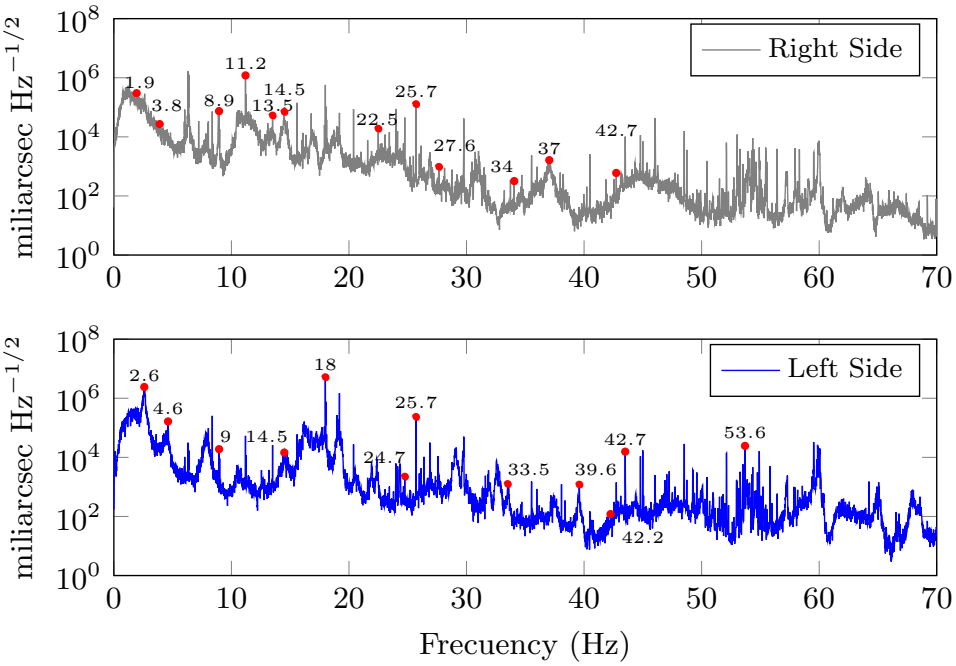

Figure 3. PSD of movement on y-axis of the focal point captured by the OVMS system.

Figure 4 and Fig. 5 show the estimated PSD of the movement on the x-axis and y-axis of the focal point captured with the WFS, respectively. Table 4 and Table 5 show the summary of the estimation of the parameters of the damped oscillators for the x-axis and y-axis, respectively.

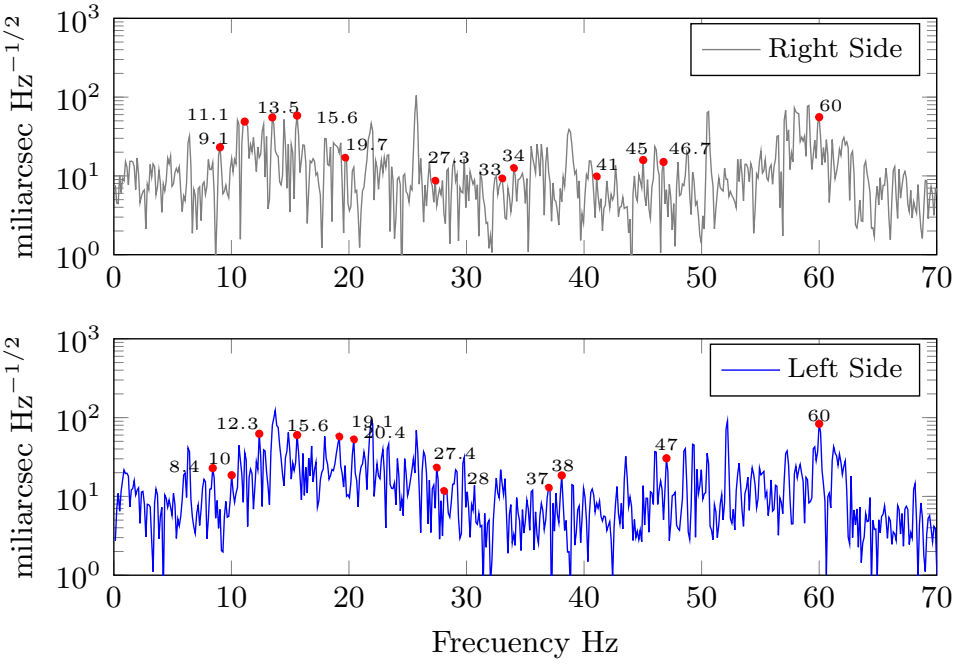

Figure 4. PSD of movement on x-axis of the focal point captured with the WFS.

Table 4. Estimation of movement on x-axis of the focal point captured with the WFS.

	Right side			Left side		
i	$\hat{\alpha}$	$\hat{\zeta}$	$\hat{\beta}$	$\hat{\alpha}$	$\hat{\zeta}$	$\hat{\beta}$
1	9.98	0.987	0.50	9.99	0.988	0.50
2	11.97	0.988	0.50	8.42	0.987	0.50
3	13.98	0.988	0.50	12.87	0.989	0.50
4	15.98	0.988	0.50	15.99	0.988	0.50
5	19.97	0.988	0.50	19.17	0.988	0.50
6	27.67	0.988	0.50	20.05	0.988	0.50
7	33.58	0.990	0.50	27.20	0.988	0.50
8	33.87	0.987	0.50	27.77	0.988	0.50
9	44.96	0.864	0.50	36.61	0.481	0.50
10	41.18	0.987	0.50	38.57	0.987	0.50
11	46.78	0.988	0.50	47.39	0.984	0.50
12	59.95	0.983	0.50	59.98	0.989	0.50

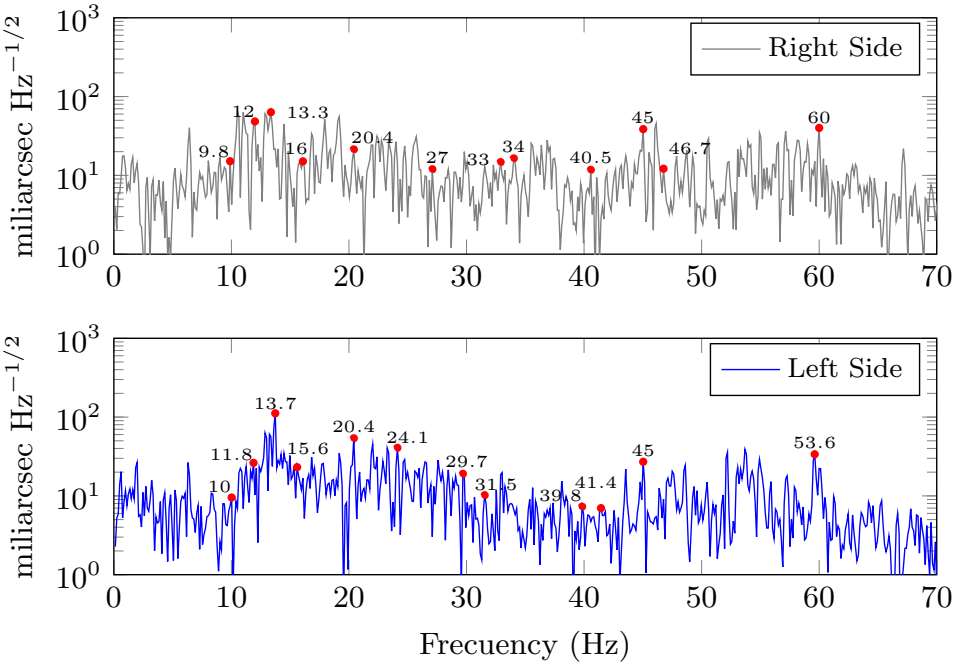

Figure 5. PSD of movement on y-axis of the focal point captured with the WFS.

Table 5. Estimation of movement on y-axis of the focal point captured with the WFS.

	Right side			Left side		
i	$\hat{\alpha}$	$\hat{\zeta}$	$\hat{\beta}$	$\hat{\alpha}$	$\hat{\zeta}$	$\hat{\beta}$
1	9.97	0.987	0.50	9.98	0.987	0.50
2	11.99	0.988	0.50	11.98	0.988	0.50
3	13.97	0.988	0.50	13.98	0.988	0.50
4	15.97	0.988	0.50	15.98	0.988	0.50
5	19.97	0.988	0.50	19.98	0.988	0.50
6	27.63	0.988	0.50	24.01	0.988	0.50
7	33.48	0.985	0.50	30.75	0.988	0.50
8	33.74	0.987	0.50	31.23	0.988	0.50
9	44.98	0.860	0.50	41.33	0.860	0.50
10	41.38	0.988	0.50	40.22	0.985	0.50
11	46.54	0.987	0.50	45.31	0.989	0.50
12	59.29	0.989	0.50	59.50	0.989	0.50

5. CONCLUSION

In this paper we proposed a novel continuos-time model for the vibrations and an ML-based technique to estimate the parameters from discrete-time samples. In the log-likelihood function we considered the parameters to estimate and the initial condition of the oscillators. The estimation was performed using local optimization, applying our method to on-sky data from the Large Binocular Telescope, which allowed us to estimate the principal peaks that arises from the estimated PSD of the system. In addition to the frequency, our method also allows to estimate the gain and the damping coefficient of the oscillators.

ACKNOWLEDGMENTS

P. Escárate thanks Núcleo Milenio de Formación Planetaria - NPF; M. coronel thanks Programa de Incentivos a la Iniciación Científica (PIIC) de la Dirección de Postgrado y Programas de la Universidad Técnica Federico Santa María (012/2018); J.C. Agüero and R. Carvajal thank Comisión Nacional de Investigación Científica y Tecnológica (CONICYT) (CONICYT-PFCHA/Doctorado Nacional/2017-21170804); Fondo Nacional de Desarrollo Científico y Tecnológico (FONDECYT) (1181158); Proyecto Basal of the Advanced Center for Electrical and Electronic Engineering (AC3E) (FB0008).

REFERENCES

1. G. Sivo, C. Kulcsár, J.-M. Conan, H.-F. Raynaud, Éric Gendron, A. Basden, F. Vidal, T. Morris, S. Meimon, C. Petit, D. Gratadour, O. Martin, Z. Hubert, A. Sevin, D. Perret, F. Chemla, G. Rousset, N. Dipper, G. Talbot, E. Younger, R. Myers, D. Henry, S. Todd, D. Atkinson, C. Dickson, and A. Longmore, "First on-sky scao validation of full lqg control with vibration mitigation on the canary pathfinder," *Opt. Express* **22**, pp. 23565–23591, Sep 2014.
2. T. Hayward, M. Ripp, H. Bonnet, C. Cavedoni, R. Galvez, G. Gausachs, and M. Cho, "Characterizing the vibration environments of the gemini telescopes," *Proceedings of the SPIE* , p. 9906:99065N, 2016.
3. M. Castro, P. Escárate, S. Zúñiga, J. Garcés, and A. Guesalaga, "Closed loop for tip-tilt vibration mitigation," in *Imaging and Applied Optics 2015*, *Imaging and Applied Optics 2015* , p. JT5A.28, Optical Society of America, 2015.
4. P. Escárate, R. Carvajal, L. Close, J. Males, K. Morzinski, and J. C. Agüero, "Minimum variance control for mitigation of vibrations in adaptive optics systems," *Applied Optics* **56**, pp. 5388–5397, Jul 2017.
5. P. Escárate, M. Coronel, K. González, R. Carvajal, and J. Agüero, "Vibration model identification using the maximum likelihood method," *Proc. SPIE 10703, Adaptive Optics Systems VI* **10703**, p. 107036R, 2018.
6. J. Lozi, O. Guyon, N. Jovanovic, N. Takato, G. Singh, B. Norris, H. Okita, T. Bando, and F. Martinache, "Characterizing vibrations at the subaru telescope for the subaru coronagraphic extreme adaptive optics instrument," *Journal of Astronomical Telescopes, Instruments, and Systems* **4**, p. 049001, 2018.
7. G. Kubin, C. Lainscsek, and E. Rank, "Identification of nonlinear oscillator models for speech analysis and synthesis," in *Nonlinear Speech Modeling and Applications: Advanced Lectures and Revised Selected Papers*, G. Chollet, A. Esposito, M. Faundez-Zanuy, and M. Marinaro, eds., pp. 74–113, Springer Berlin Heidelberg, Berlin, Heidelberg, 2005.
8. J. Garcés, S. Zúñiga, L. Close, J. Males, K. Morzinski, P. Escárate, M. Castro, J. Marchioni, and D. Rojas, "Vibrations in magao: resonance sources identification and first approaches for modeling and control," *Proceedings SPIE* **9909**, pp. 9909 – 9909 – 17, 2016.
9. S. Zúñiga, J. Garcés, L. Close, J. Males, K. Morzinski, P. Escárate, M. Castro, J. Marchioni, and D. R. Zagals, "Vibrations in magao: frequency-based analysis of on-sky data, resonance sources identification, and future challenges in vibrations mitigation," *Proceedings SPIE* **9909**, pp. 9909 – 9909 – 6, 2016.
10. G. E. P. Box, G. M. Jenkins, G. C. Reinsel, and G. M. Ljung, *Time series analysis: forecasting and control*, John Wiley & Sons, Hoboken, New Jersey, USA, 5th ed., 2016.
11. K. González, M. Coronel, R. Carvajal, P. Escárate, and J. Agüero, "Maximum likelihood identification of a continuous-time oscillator utilizing sampled data," *IFAC Symposium on System Identification (SYSID)* **18**, p. 712–717, 2018.

12. T. Söderström, *Discrete-Time Stochastic Systems: Estimation and Control*, Springer-Verlag New York, Inc., Secaucus, NJ, USA, 2002 (second edition).
13. F. Chen, J. C. Agüero, M. Gilson, H. Garnier, and T. Liu, "EM-based identification of continuous-time ARMA models from irregularly sampled data," *Automatica* **77**(3), pp. 293 – 301, 2017.
14. A. Prior and P. de Oliveira, "Parameter estimation of a two regime stochastic differential model for a bilinear oscillator subjected to random loads," *Proc. of the 9th International Conference on Structural Dynamics, EURODYN 2014* , pp. 2845–2852, 30 June - 2 July 2014.
15. M. Kürster, T. Bertram, J. L. Borelli, M. Brix, W. Gässler, T. M. Herbst, V. Naranjo, J.-U. Pott, J. Trowitzsch, T. E. Connors, P. M. Hinz, T. J. McMahon, D. S. Ashby, J. G. Brynnel, N. J. Cushing, T. Edgin, J. D. Esguerra, R. F. Green, J. Kraus, J. Little, U. Beckmann, and G. P. Weigelt, "Ovms: the optical path difference and vibration monitoring system for the lbt and its interferometers," *Proceedings SPIE* **7734**, pp. 7734 –7734 – 8, 2010.
16. M. Böhm, J.-U. Pott, J. Borelli, P. Hinz, D. Defrère, E. Downey, J. Hill, K. Summers, A. Conrad, M. Kürster, T. Herbst, and O. Sawodny, "Ovms-plus at the lbt: disturbance compensation simplified," *Proceedings SPIE* **9906**, pp. 9906 – 9906 –8, 2016.
17. R. Byrd, J. Gilbert, and J. Nocedal, "A trust region method based on interior point techniques for nonlinear programming," *Mathematical Programming* **89**(1), p. 149–185, 2000.